IEEE Photonics Journal
An IEEE Photonics Society Publication

Open Access

Employing Microwave Graphene Field Effect Transistors for Infrared Radiation Detection

Volume 10, Number 2, April 2018

Antonio Benfante
Marco A. Giambra
Riccardo Pernice
Salvatore Stivala
Enrico Calandra
Antonino Parisi
Alfonso C. Cino
Simone Dehm
Romain Danneau
Ralph Krupke
Alessandro C. Busacca

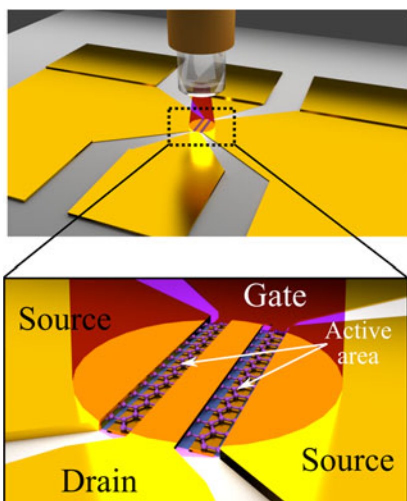

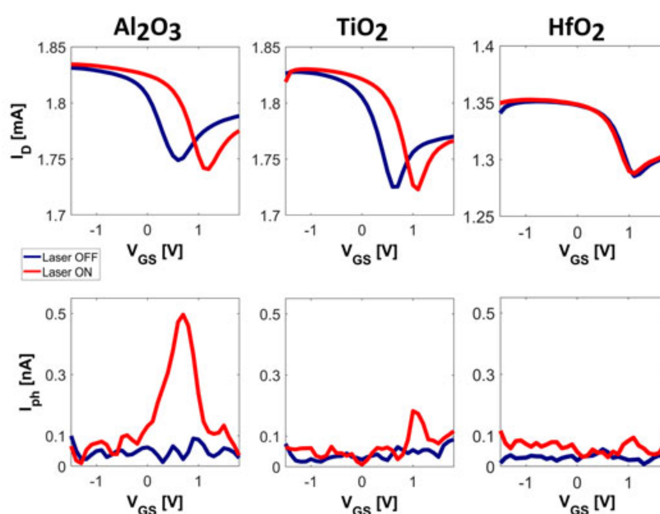

DOI: 10.1109/JPHOT.2018.2807923
1943-0655 © 2018 IEEE

IEEE photonics SOCIETY
IEEE

Employing Microwave Graphene Field Effect Transistors for Infrared Radiation Detection

Antonio Benfante,[1†] **Marco A. Giambra**,[2†] **Riccardo Pernice**,[1] **Salvatore Stivala**,[1] **Enrico Calandra**,[1] **Antonino Parisi**,[1] **Alfonso C. Cino**,[1] **Simone Dehm**,[3] **Romain Danneau**,[3] **Ralph Krupke**,[3,4] **and Alessandro C. Busacca**[1]

[1]Department of Energy, Information engineering and Mathematical models (DEIM), University of Palermo, Palermo 90128, Italy
[2]CNIT – Consorzio Nazionale Interuniversitario per le Telecomunicazioni, Pisa 43124, Italy
[3]Institute of Nanotechnology, Karlsruhe Institute of Technology, Karlsruhe 76021, Germany
[4]Institute of Materials Science, Technische Universität Darmstadt, Darmstadt 64287, Germany
[†]These authors contributed equally to this manuscript.

DOI:10.1109/JPHOT.2018.2807923
1943-0655 © 2018 IEEE. Translations and content mining are permitted for academic research only. Personal use is also permitted, but republication/redistribution requires IEEE permission. See http://www.ieee.org/publications_standards/publications/rights/index.html for more information.

Manuscript received January 22, 2018; revised February 13, 2018; accepted February 15, 2018. Date of publication February 21, 2018; date of current version March 6, 2018. Corresponding author: A. Benfante (E-mail: antonio.benfante@unipa.it).

Abstract: In this work, we investigate the possibility of employing graphene field effect transistors, specifically designed for microwave applications, as infrared detectors for telecom applications. Our devices have been fabricated on a sapphire substrate employing CVD-grown transferred graphene. The roles of both the gate dielectric and the DC bias conditions have been evaluated in order to maximize the infrared generated signal through an experimental investigation of the signal-to-noise ratio dependence on the transistor operating point.

Index Terms: Graphene, graphene field effect transistors, infrared detectors, microwave transistors.

1. Introduction

Due to its unique electronic, optical, thermal and mechanical properties, graphene has attracted a huge attention from both the academic and the industrial communities. Thanks to its peculiar features – such as extremely high charge carrier mobility, broadband light absorption, very fast carrier dynamics, theoretical sheet resistance of 30 Ω/□, high fracture resistance and chemical stability – graphene has already been extensively applied in flexible electronics and energy conversion devices, such as touch screens, Field-Effect Transistors (FETs), capacitors, batteries, solar cells and Light-Emitting Diodes (LEDs) [1], [2]. Graphene multifunctionality has also been further demonstrated in the last years, with graphene-based composites employed for light-controlled conductive switching fabrication [3] and in-vivo bioimaging [4]. In graphene-based devices, photovoltaic [5]–[8], photothermoelectric [9]–[11] and bolometric [8], [12] effects have been proved to be the main mechanisms involved in light detection, giving the opportunity of employing graphene as a possible substitute to more conventional photodetectors materials [1], [13], [14]. Different approaches have been already proposed for the fabrication of such devices using monolayer graphene alongside

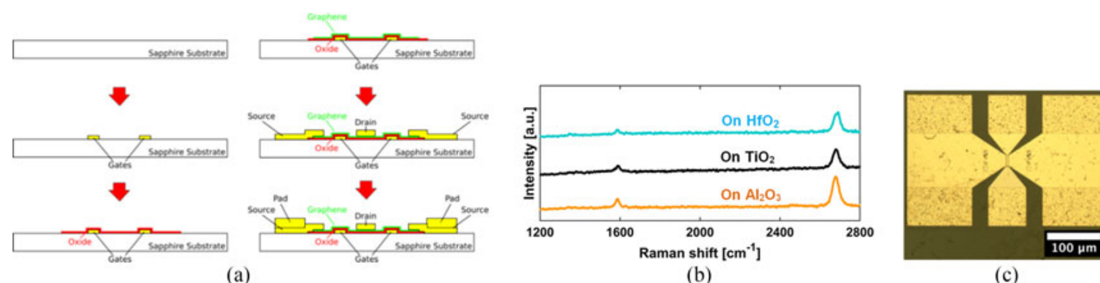

Fig. 1. (a) GFETs fabrication steps and (b) comparison among Raman spectra of transferred graphene on top of the different dielectrics. (c) Micrograph of a fabricated device.

metals or semiconductors [15]–[18]. In particular, silicon has been widely employed as substrate and back gate material, while dielectric layers have been traditionally fabricated using SiO_2 [9]–[12].

In this work, we investigate the possibility of employing Graphene Field Effect Transistors (GFETs), specifically designed for microwave applications, to sense infrared radiation. As expected, since our transistors have been conceived to optimize microwave performance, a lower responsivity, if compared to conventional graphene-based IR detectors, has been found [19]. Nevertheless, this approach gives us the opportunity to exploit graphene multifunctionality. In particular, the proposed device is able to sense the incoming 1.55 μm wavelength radiation and amplify the generated electrical signal: this makes our GFETs suitable for telecom applications. In this work, we also study the influence of the gate dielectric on IR photoresponse, evaluating the signal-to-noise ratio as a function of transistors bias point. Aluminum oxide (Al_2O_3), titanium oxide (TiO_2) and hafnium oxide (HfO_2) have been chosen because they show quite different electric and thermal properties and can be easily deposited through Atomic Layer Deposition (ALD) systems.

2. Phototransistors Fabrication

The transistors have been realized on a sapphire substrate [20] employing a dual bottom-gate geometry [see Fig. 1(a)]. First, the dual-finger back-gate was patterned on the substrate by e-beam lithography followed by the evaporation of a thin Ti/Au bilayer ($\sim$5/40 nm) and lift-off in acetone [21]. In order to study the role of the gate oxides, $\sim$10 nm thick Al_2O_3, TiO_2 and HfO_2 films have been directly grown via ALD on different areas of the same chip and used as gate dielectrics. Subsequently, a CVD-grown monolayer graphene film was directly transferred onto the chip. Afterwards, graphene has been patterned in a meander geometry by Reactive Ion Etching (RIE) to minimize contact resistance [22]. After transfer, Raman spectroscopy has been employed to assess the high quality and single-layer nature of the transferred graphene on top of the three oxides, as shown by the distinctive G (1580 cm^{-1}) and 2D (2680 cm^{-1}) peaks reported in Fig. 1(b). Then, source/drain electrodes have been realised onto the graphene sheet using e-beam lithography followed by a Ti/Au ($\sim$5/100 nm) deposition and lift-off in acetone. Finally, $\sim$300 nm-thick Au contact pads have been directly deposited by PVD. A micrograph of a fabricated device is shown in Fig. 1(c).

3. Measurements Set-Up

Photoelectrical measurements have been performed at room temperature using a 1.55 μm erbium fiber laser (IPG Photonics ELT-1-CL-SF-LP) with the output beam chopped at 667 Hz and coupled into a single mode optical fiber through a microscope objective (Edmund DIN 20). The GFETs electrical output voltage has been measured using a lock-in amplifier (Stanford Research Systems SR830) synchronized to the chopper frequency. Dedicated software has been developed

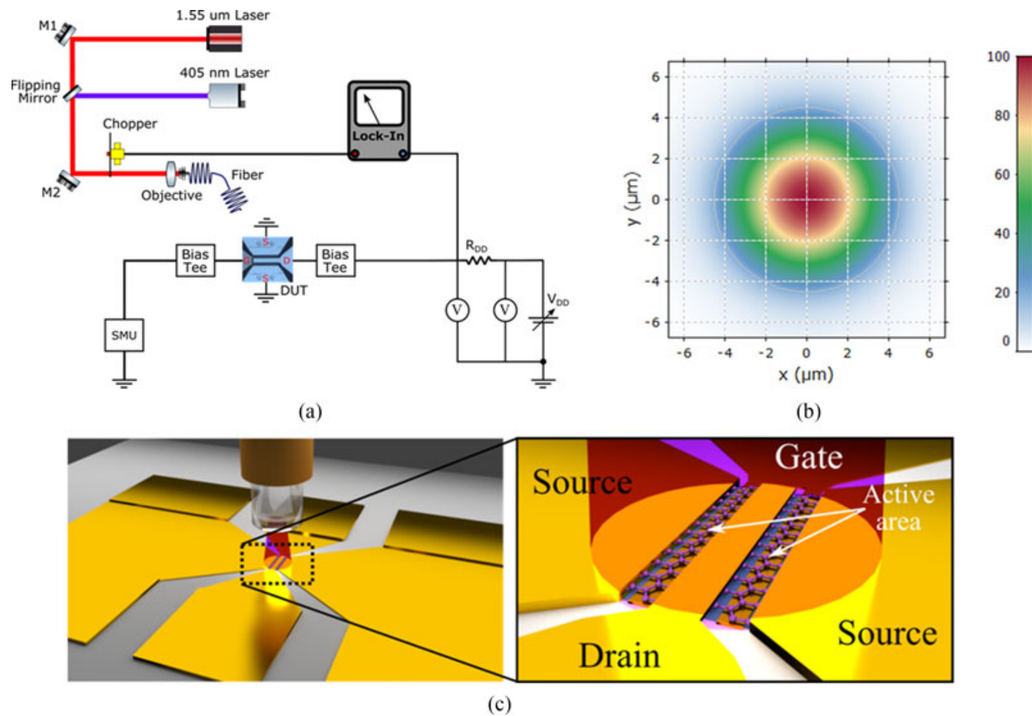

Fig. 2. (a) Schematic of the experimental setup for optical measurements, where M1-M2 are mirrors, DUT is the Device Under Test and SMU is the Source-Meter Unit employed for GFET gate bias. Drain bias, instead, has been applied through a battery-resistance (V_{DD}-R_{DD}) combination. (b) Intensity plot of the simulated beam after exiting the fiber. (c) Sketch of the GFET under laser illumination.

to automate the DC/optical measurements bench. A sketch of the experimental set-up is depicted in Fig. 2(a).

An auxiliary visible laser (405 nm laser diode) has been employed for alignment purpose and kept off during the subsequent IR characterization, while a DC Source-Meter Unit (SMU) has been used for the device gate bias. The drain bias, instead, has been applied through a battery-resistance (V_{DD}–R_{DD}) combination. This arrangement allowed to reduce the low-frequency AC noise level with respect to the one typically associated to a digital SMU and to develop the desired optically-induced AC signal to drive the lock-in amplifier. Two additional voltmeters have also been employed to measure the voltage drop both upstream and downstream of the R_{DD} resistance. Starting from the single mode optical fiber specifications, we analytically evaluated the spot size (w) of the IR beam at its output facet, obtaining a value of $w = 5.3\ \mu m$ [see Fig. 2(b)] [23]. Then, the laser spot area on the sample (0.065 mm^2) has been calculated by simulating the free space propagation of the beam exiting the fiber for a distance of ~1.5 mm (i.e., the distance between the fiber end and the sample) and irradiating the 40-μm^2 graphene active area [see Fig. 2(c)].

4. Results and Discussion

Our analysis has been performed to find out the maximum GFETs IR responsivity, varying both the DC operating point and the gate dielectric. For our analysis, typical bias voltages for graphene-based high frequency transistors have been chosen [20]. In particular, the drain-source voltage has been varied between 0.06 V and 1 V, while the gate-source voltage in the range from −1.5 V to 1.5 V. In what follows, we refer to signal as the maximum drain-source photocurrent (i.e., I_{ph}) generated under laser irradiation, and to noise as the mean value of the lock-in current with no laser excitation (I_n). The drain-source photocurrent has been calculated as the ratio between the

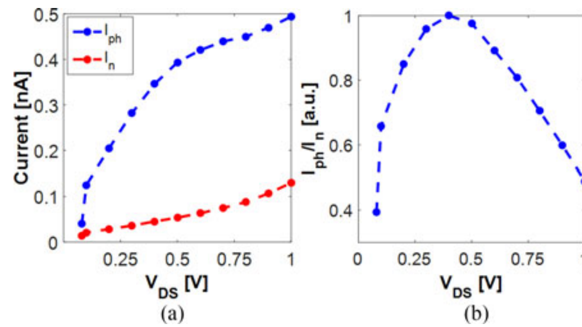

Fig. 3. (a) I_{ph}, I_n and (b) normalized I_{ph}/I_n as function of V_{DS} for devices employing Al_2O_3 as gate dielectric, at $V_{GS} = 0.7$ V. The laser power on the sample was set to 7 mW.

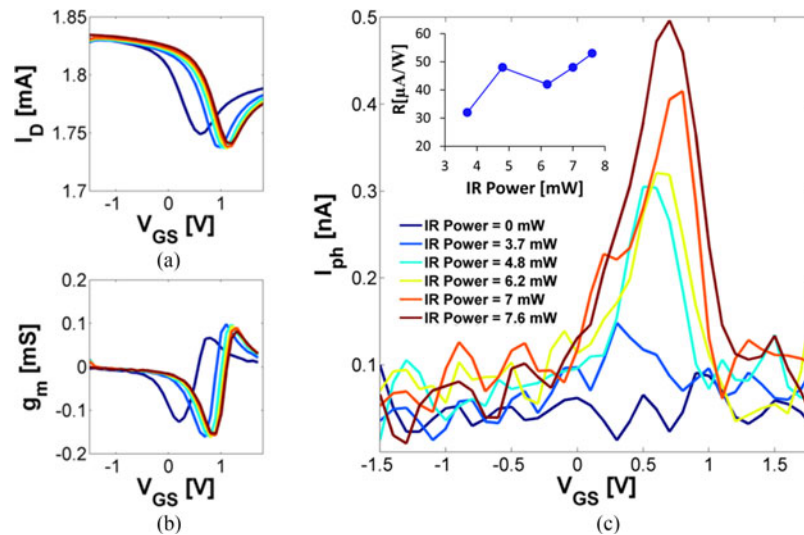

Fig. 4. (a) Static drain current, (b) static transconductance and (c) photocurrent vs. gate source voltage (V_{GS}) under different IR power irradiation. Inset: Peak responsivity versus IR laser power at $V_{DS} = 0.4$ V.

voltage acquired by the lock-in amplifier and the R_{DD} resistance shown in Fig. 2(a). In the case of Al_2O_3 based devices, the dependence of I_{ph}, I_n and I_{ph}/I_n on the drain-source voltage is depicted in Fig. 3.

From Fig. 3(a), we notice an initial increase of the photocurrent (blue curve) with the V_{DS} value, followed by a saturation starting at $V_{DS} \sim 0.5$ V. We assume this behavior to be related to the non-linear gain characteristics associated with the active (transistor) nature of our devices, unlike it happens with more conventional passive photodetectors. Noise (red curve), instead, rises with V_{DS}, with an approximately linear trend on the entire explored bias range, leading to a maximum I_{ph}/I_n ratio at $V_{DS} = 0.4$ V [see Fig. 3(b)]. The subsequent analysis of GFETs photoelectrical response as a function of the laser power impinging on the devices, in the range [0–7.6] mW, has been performed at such voltage. More precisely, static drain-source current [I_D, see Fig. 4(a)], static transconductance [$g_m = \partial I_D/\partial V_{GS}|_{VDS=const}$, see Fig. 4(b)] and photocurrent [I_{ph}, see Fig. 4(c)] have been measured simultaneously.

The obtained results demonstrate that photocurrent [see Fig. 4(c)] increases with the laser power, reaching its peak value ($I_{ph} = 0.49$ nA) close to the Dirac point, in particular at the gate bias in which the I_D–V_{GS} curve has its maximum slope, i.e., the magnitude of the static transconductance is maximum ($g_m = -0.15$ mS) [see Fig. 4(b)]. As it can be noticed [see Fig. 4(a)], static drain

currents shift according to the laser power impinging on the sample, as found in photogating-dominated detectors [24]. The peak photodetector responsivity (R) has also been calculated as the ratio between the peak generated photocurrent ($I_{ph,peak}$) and the optical power impinging the graphene active area [40-μm^2, see Fig. 2(c)]. Taking into account the Gaussian distribution of the beam intensity, R becomes:

$$R = \frac{I_{ph,peak}}{Optical\ Power} = \frac{I_{ph,peak}}{\frac{2P}{\pi w^2}\left(\iint_{\substack{Active\\Area}} e^{-2\frac{x^2+y^2}{w^2}}dxdy\right)} \quad (1)$$

where w is the beam waist (1/e^2 radius, 145 μm in our case) and P is the value of the optical power on the sample. For $V_{DS} = 0.4$ V, the responsivity reaches its maximum value (~53 μA/W) at the maximum optical power tested (7.6 mW). In fact, as depicted in the inset of Fig. 4(c), the responsivity shows an upward trend.

As expected, measured maximum responsivity is lower if compared to conventional graphene-based IR detectors due to the microwave-oriented design of our devices [19] which is not optimized for radiation detection. In fact, it has to be pointed out that the ~2.3% single layer graphene absorption already reported in the literature, although impressive for a one–atom thick material, is not sufficient for competitive photodetection applications. Moreover, the zero bandgap nature, essential for broadband detection, leads to a short lifetime of excitons, which is unfavorable for the exciton separation itself. These characteristics cause the responsivity values of pure single layer graphene to be limited to a few mA/W [19]. In our case, even worse values are awaited due to the reduced exposed graphene area and large metal electrodes needed to properly inject and extract the RF signal. However, higher responsivity values can be expected by employing *ad hoc* optical structures that help the photons confinement or by the functionalization of the graphene layer. Nevertheless, these solutions can come at the expense of the operation speed, so a trade-off needs to be found with RF response. However, further improvement on the overall performance (RF and optical) of the proposed devices can be reasonably obtained by adopting single-crystal CVD graphene and optimized transfer. As to the mechanisms of photogeneration involved in our GFETs, it can be explained as follows. The optical signal is first down-converted to an electrical signal and, then, amplified exploiting the transistor effect of our devices. It is also evident that the substrate is not able to provide charge carriers, given the higher energy bandgap of sapphire (7.3 eV) compared to the incident laser energy (0.8 eV). The same characterization has also been performed on TiO_2 and HfO_2 based devices, finding lower photocurrents and I_{ph}/I_n ratios than those measured for Al_2O_3 samples. Fig. 5 compares the photoresponse of GFETs employing the three different gate dielectrics, together with the corresponding static curves. Drain-source voltage values have been chosen to maximize the I_{ph}/I_n ratio. Optical measurements show that transistors employing Al_2O_3 exhibit the highest photocurrent value when $V_{GS} = 0.7$ V, followed by those devices that make use of TiO_2. No photoresponse, instead, has been detected in samples with HfO_2, independently on the DC operating point chosen. As it can be noticed, a wrong choice of the transistor operating point can strongly compromise the photodetector performance and only proper DC bias conditions ensure a sharp variation of the output photocurrent as a function of the input optical signal.

As it can be observed comparing static drain currents with (red curves) and without (blue curves) laser power shining on the samples [see Fig. 5(a), (b), (c)], Dirac points shift with increasing illumination only for Al_2O_3 and TiO_2 based samples. On the other hand, no considerable shifts are found for those samples employing HfO_2 as gate dielectric. In other words, we notice a correlation between photocurrent and photo-induced shifts of static drain currents, which we believe to be in favor of photogating effect. The spatial distribution of surface or interfaces trap states, in fact, has been reported to cause the above-mentioned horizontal shifts. Under laser irradiation, trap states can trap photo-generated carriers whose accumulation induces a gate electric field leading to a modulation of the channel conductance [24]. The analysis of both the static drain currents and the photoresponses of our devices allows us to conclude that different interface/trap states configurations are created after transferring graphene on top of the three dielectrics and that the

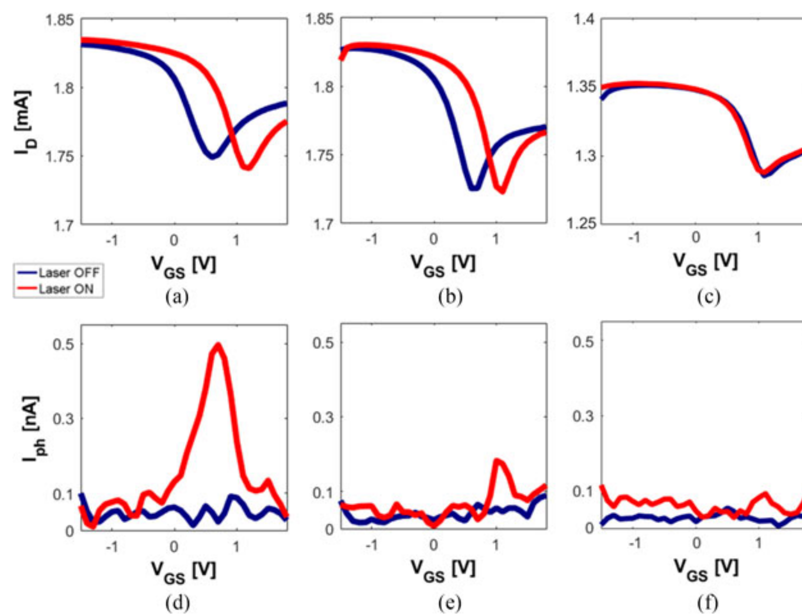

Fig. 5. Static drain current (I_D) and photocurrent (I_{ph}) vs. gate-source voltage (V_{GS}) for GFETs employing (a, d) Al_2O_3 (at $V_{DS} = 0.4$ V), (b, e) TiO_2 (at $V_{DS} = 0.1$ V) and (c, f) HfO_2 (at $V_{DS} = 0.2$ V) as gate oxide, with (red curves) and without (blue curves) laser power impinging on the samples at 7.6 mW.

use of Al_2O_3 as gate oxide gives rise to a more effective modulation of the channel conductance under laser irradiation and, consequently, to a higher photocurrent.

5. Conclusion

In this paper, graphene-based microwave transistors have been used for IR detection. Although a lower responsivity is expected than conventional graphene photodetector, the proposed device is able both to sense the incoming 1.55 μm radiation and amplify the photogenerated electrical signal making it suitable for telecom application. An in-depth analysis of the influence of both the DC transistors operating point and the gate oxide on the IR photoresponse has been performed to optimize detector responsivity without penalizing transistor microwave performance. The best results have been obtained at $V_{DS} = 0.4$ V and a maximum photoresponsivity of $\sim$53 μA/W at room temperature has been found for devices employing Al_2O_3.

References

[1] A. C. Ferrari *et al.*, “Science and technology roadmap for graphene, related two-dimensional crystals, and hybrid systems,” *Nanoscale*, vol. 7, no. 11, pp. 4598–4810, 2015.

[2] M. H. Griep, E. Sandoz-Rosado, T. M. Tumlin, and E. Wetzel, “Enhanced graphene mechanical properties through ultrasmooth copper growth substrates,” *Nano Lett.*, vol. 16, no. 3, pp. 1657–1662, 2016.

[3] J. Wei, Z. Zang, Y. Zhang, M. Wang, J. Du, and X. Tang, “Enhanced performance of light-controlled conductive switching in hybrid cuprous oxide/reduced graphene oxide (Cu_2O/rGO) nanocomposites,” *Opt. Lett.*, vol. 42, pp. 911–914, 2017.

[4] Z. Zang, X. Zeng, M. Wang, W. Hu, C. Liu, and X. Tang, “Tunable photoluminescence of water-soluble AgInZnS–graphene oxide (GO) nanocomposites and their application in-vivo bioimaging,” *Sensors Actuators B*, vol. 252, pp. 1179–1186, 2017.

[5] E. C. Peters, E. J. H. Lee, M. Burghard, and K. Kern, “Gate dependent photocurrents at a graphene p–n junction,” *Appl. Phys. Lett.*, vol. 97, pp. 193102-1–193102-3, 2010.

[6] G. Rao, M. Freitag, H-Y. Chiu, R. S. Sundaram, and P. Avouris, “Raman and photocurrent imaging of electrical stress-induced p–n Junctions in graphene,” *ACS Nano*, vol. 5, no. 7, pp. 5848–5854, 2011.

[7] T. Mueller, F. Xia, M. Freitag, J. Tsang, and Ph. Avouris, “Role of contacts in graphene transistors: A scanning photocurrent study,” *Phys. Rev. B*, vol. 79, pp. 245430-1–245430-6, 2009.

[8] M. Freitag, T. Low, F. Xia, and P. Avouris, "Photoconductivity of biased graphene," *Nature Photon.*, vol. 7, pp. 53–59, 2013.
[9] N. M. Gabor *et al.*, "Hot carrier–assisted intrinsic photoresponse in graphene," *Science*, vol. 334, no. 6056, pp. 648–652, 2011.
[10] Y. Shi, W. Fang, K. Zhang, W. Zhang, and L-J. Li, "Photoelectrical response in single-layer graphene transistors," *Small*, vol. 5, no. 17, pp. 2005–2011, 2009.
[11] X. Xu, N. M. Gabor, J. S. Alden, A. M. van der Zande, and P. L. McEuen, "Photo-thermoelectric effect at a graphene interface junction," *Nano Lett.*, vol. 10, no. 2, pp. 562–566, 2010.
[12] M.-H. Kim, J. Yan, R. J. Suess, T. E. Murphy, M. S. Fuhrer, and H. D. Drew, "Photothermal response in dual-gated bilayer graphene," *Phys. Rev. Lett.*, vol. 110, no. 24, 2013, Art. no. 247402.
[13] F. H. L. Koppens, T. Mueller, P. Avouris, A. C. Ferrari, M. S. Vitiello, and M. Polini, "Photodetectors based on graphene, other two-dimensional materials and hybrid systems," *Nature Nanotechnol.*, vol. 9, pp. 780–793, 2014.
[14] F. Bonaccorso, Z. Sun, T. Hasan, and A. C. Ferrari, "Graphene photonics and optoelectronics," *Nature Photon.*, vol. 4, pp. 611–622, 2010.
[15] E. J. H. Lee, K. Balasubramanian, R. T. Weitz, M. Burghard, and K. Kern, "Contact and edge effects in graphene devices," *Nature Nanotechnol.*, vol. 3, pp. 486–490, 2008.
[16] F. Xia *et al.*, "Photocurrent imaging and efficient photon detection in a graphene transistor," *Nano Lett.*, vol. 9, no. 3, pp. 1039–1044, 2009.
[17] X. Li, H. Zhu, K. Wang, A. Cao, J. Wei, C. Li, Y. Jia, Z. Li, X. Li, and D. Wu, "Graphene-on-silicon Schottky junction solar cells," *Adv. Mater.*, vol. 22, no. 25, pp. 2743–2748, 2010.
[18] S. Tongay, M. Lemaitre, X. Miao, B. Gila, B. R. Appleton, and A. F. Hebard, "Rectification at graphene–semiconductor interfaces: Zero-gap semiconductor-based diodes," *Phys. Rev. X*, vol. 2, no. 1, pp. 011002-1–011002-10, 2012.
[19] Z. Sun and H. Chang, "Graphene and graphene-like two-dimensional materials in photodetection: Mechanism and methodology," *ACS Nano*, vol. 8, no. 5, pp. 4133–4156, 2014.
[20] E. Pallecchi, C. Benz, A. C. Betz, H. Löhneysen, B. Plaçais, and R. Danneau, "Graphene microwave transistors on sapphire substrates," *Appl. Phys. Lett.*, vol. 99, pp. 113502-1–113502-3, 2011.
[21] C. Benz *et al.*, "Graphene on boron nitride microwave transistors driven by graphene nanoribbon back-gates," *Appl. Phys. Lett.*, vol. 102, pp. 033505-1–033505-4, 2013.
[22] J. T. Smith, A. D. Franklin, D. B. Farmer, and C. D. Dimitrakopoulos, "Reducing contact resistance in graphene devices through contact area patterning," *ACS Nano*, vol. 7, no. 4, pp. 3661–3667, 2013.
[23] G. P. Agrawal, *Fiber-Optic Communications Systems.* New York, NY, USA: Wiley, 2002, ch. 2.
[24] H. Fang and W. Hu, "Photogating in low dimensional photodetectors," *Adv. Sci.*, vol. 4, no. 12, pp. 1700323-1–1700323-17, 2017.